Gate-modulated generation–recombination current in n-type metal–oxide–semiconductor field-effect transistor*

Chen Hai-Feng(陈海峰)†

School of Electronic Engineering, Xi'an University of Posts and Telecommunications, Xi'an 710121, *China*

(Received 5 June 2014; revised manuscript received 17 July 2014; published online 20 October 2014)

Gate-modulated generation–recombination (GMGR) current I_{GMGR} induced by the interface traps in an n-type metal–oxide–semiconductor field-effect transistor (nMOSFET) is investigated. The generation current is found to expand rightwards with increasing the reversed drain PN junction bias, and the recombination current is enhanced as the forward drain bias increases. The variations of I_{GMGR} curves are ascribed to the changes of the electron density and hole density at the interface, N_S and P_S, under the different drain bias voltages. Based on an analysis of the physical mechanism, the I_{GMGR} model is set up by introducing two coefficients (m and t). The coefficients m and t can modulate the curves widths and peak values. The simulated results under reverse mode and forward mode are obviously in agreement with the experimental results. This proves that this model can be applicable for generation current and recombination current and that the theory behind the model is reasonable. The details of the relevant mechanism are given in the paper.

Keywords: generation, recombination, interface trap, nMOSFET

PACS: 85.30.De, 85.30.Tv **DOI:** 10.1088/1674-1056/23/12/128502

1. Introduction

The Si/SiO_2 interface in a metal–oxide–semiconductor field-effect transistor (MOSFET) is a very critical region and affects the electrical performance of the device.[1] The interface traps can serve as the generation–recombination centers when the channel depletion region is in the non-equilibrium condition.[2,3] The gate voltage U_G results in the change of surface potential and then makes the electron density N_S and the hole density P_S around the interface vary. So a weak current forms under this modulation of U_G, and this current is called the gate-modulated generation–recombination (GMGR) current I_{GMGR}. As this current is very sensitive to the interface traps and has the potential to be utilized in the development of new devices, it has received a great deal of attention in recent years. Mori *et al.*[4] ascribed the dynamic drain PN junction leakage in MOSFET to the fluctuation of the interface generation current. Young *et al.*[5] studied the influence of the temperature stress on the generation current in the high K gate dielectric. Bina *et al.*[6] also studied the temperature stress on the interface and set up a multistate multi-phonon model for the recombination current in MOSFET. Chen *et al.*[7] and Chen[8] discussed the transconductance of the generation current and the effect of substrate bias modulating the generation current. The characteristics of the generation current in a fin field-effect transistor (FinFET) were studied by Zhang *et al.*,[9] and Ma *et al.*[10] obtained the model of the damage distribution at the interface in FinFET using the recombination current method. Additionally, Zhang *et al.*[11] extracted the value of substrate doping concentration and the thickness of gate oxide on the bases of the recombination current.

Although many researches have been conducted, the interfacial electronic traps in the control of gate are not understood completely. The interface traps under the gate show the generation and recombination effects and result in two currents. So it is necessary to seek the physical mechanisms of generation and recombination current and set up the models which can acutely describe them.

In this paper, we study the characteristics of I_{GMGR} under the reverse and forward drain PN junction modes. Through analyzing the I_{GMGR} curves with various values of drain biase voltage U_D, the physical mechanism of interface-trap-induced generation–recombination current is discussed deeply and the relevant model is set up.

2. Experiment and device

The device used in this study was an nMOSFET with the n+ poly-Si gate fabricated by 90-nm complementary-metal–oxide–semiconductor (CMOS) technology. The gate oxide with a thickness (t_{ox}) of 4 nm was fabricated through the decoupled-plasma-nitridation process. The gate length (l) was 0.28 μm, and the gate width (w) was 6 μm. For the measurement, floating the source and grounding the substrate, the gate was controlled using a swept voltage from a source monitor unit (SMU) and was swept from accumulation to strong inversion ($-0.4\ \text{V} < U_G < 1.0\ \text{V}$). The reverse drain PN bias U_D values were 0.05 V, 0.1 V, 0.2 V, 0.3 V, and 0.4 V for the gener-

*Project supported by the National Natural Science Foundation of China (Grant No. 61306131) and the Research Project of Education Department of Shaanxi Province, China (Grant No. 2013JK1095).

†Corresponding author. E-mail: chenhaifeng@xupt.edu.cn

© 2014 Chinese Physical Society and IOP Publishing Ltd

ation current measurement, and the forward drain PN bias U_D values were -0.05 V and -0.1 V for the recombination current measurement. Then the current collected by the drain was I_{GMGR}. All electrical tests were performed by using a Keithley 4200 precision semiconductor parameter analyzer.

3. Results and discussion

Figure 1(a) shows the I_{GMGR}–U_G curves at the reverse and forward measurement modes. In the case of the reverse drain PN junction bias mode ($U_D > 0$), I_{GMGR} is the generation current, in fact. In this mode, the generation current is enhanced as U_G increases from accumulation, the flat band voltage U_{FB}, to depletion, and the I_{GMGR} curves start to go up. Afterwards, these curves drop off quickly when U_G is beyond the threshold voltage U_{TH}, as seen in Fig. 1(a). It is found that the peak of the I_{GMGR} curve augments as U_D increases from 0.05 V to 0.2 V. When $U_G > 0.2$ V, the I_{GMGR} curve peak keeps constant and the width of the curve expands. But in the other case of the forward drain PN junction bias mode ($U_D < 0$), I_{GMGR} is negative because it contains recombination current at this time. It can be seen that the recombination current peak increases and the I_{GMGR} curve shifts leftwards as U_D increases from -0.05 V to -0.1 V. Figure 1(b) shows that the drain current I_{GMGR} is almost zero at $U_D = 0$ V with U_G increasing from accumulation, depletion to inversion. This indicates that there is no generation–recombination current without the assistance of the drain bias U_D. In other words, it proves that U_D dominates the formation of generation and recombination currents in Fig. 1(a).

The role of U_D in the I_{GMGR} curves is mainly to modulate the electron density N_S and hole density P_S in Si around the interface. U_D causes the minority carrier (electron) quasi-Fermi level E_{FN} to be reduced by about the magnitude of qU_D but has no influence on the majority carrier (hole) quasi-Fermi level E_{FP}. So the expressions of N_S and P_S are obtained as $N_S = n_0 \exp[\beta(\varphi_S – U_D)]$, and $P_S = p_0 \exp(-\beta\varphi_S)$. In these expressions, $\beta = q/kT$, with k being the Boltzmann constant, T the temperature and φ_S the surface potential; n_0 and p_0 are the electron density and the hole density in an equilibrium state, respectively. For p-type Si substrate, p_0 is equal to N_A. As φ_S is very close to U_G and U_D, they are related by $U_G = U_{FB} + \varphi_S + U_{ox}$.[12] As U_D can increase the depletion width and consequently change the voltage drops of gate oxide U_{ox}, the above equation can be rewritten as

$$U_{GF} = \varphi_S + [2q\varepsilon_s N_A(\varphi_S + U_D)]^{1/2}/C_{ox}, \tag{1}$$

where C_{ox} is the gate capacitance and $U_{GF} = U_G - U_{FB}$.

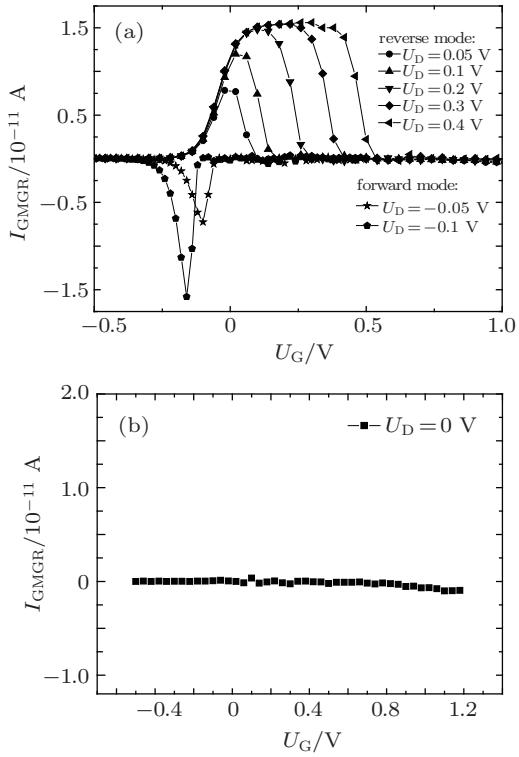


Fig. 1. Variations of experimental I_{GMGR} with gate voltage U_G at (a) $U_D \neq 0$ V for both reverse and forward drain PN junction biases, and (b) $U_D = 0$ V.

Then substituting Eq. (1) into the expressions of N_S an P_S above, the relationship of N_S and P_S with U_G and U_D can be described as

$$N_S(U_G, U_D) = n_0 \exp\left\{\beta\left[\frac{q\varepsilon_s N_A}{C_{ox}^2} + U_{GF} - \frac{(2q\varepsilon_s N_A)^{1/2}}{C_{ox}} \times \sqrt{\frac{q\varepsilon_s N_A}{2C_{ox}^2} + U_{GF} + U_D} - U_D\right]\right\},$$

$$P_S(U_G, U_D) = N_A \exp\left\{-\beta\left[\frac{q\varepsilon_s N_A}{C_{ox}^2} + U_{GF} - \frac{(2q\varepsilon_s N_A)^{1/2}}{C_{ox}} \times \sqrt{\frac{q\varepsilon_s N_A}{2C_{ox}^2} + U_{GF} + U_D}\right]\right\}. \tag{2}$$

According to Eq. (2), figure 2 shows the simulated curves of N_S and P_S versus U_{GF} at various U_D values. In the figure, P_S decreases and N_S increases with increasing U_{GF}. Note that P_S almost keeps constant but the N_S curve shifts distinctly rightwards as U_D increases. Moreover, all the crossover points of N_S and P_S curves are located at $U_{GF} > 0$ V, which shows that the channel is in depletion.

N_S and P_S determine the generation–recombination rate G, which reads[13,14]

$$G = \frac{n_i^2 - N_S P_S}{N_S + P_S + 2n_i ch[(E_t - E_i)/kT]}. \tag{3}$$

For simplicity, it is assumed that generation–recombination center is located at the mid-gap energy position, i.e., at $E_t = E_i$. Substituting Eq. (2) into Eq. (3), G becomes

$$G(P_S, N_S) = A(U_D) \times B(U_G, U_D) \times n_i^2, \tag{4}$$

$$A(U_D) = [1 - \exp(-\beta U_D)], \quad (5)$$

$$B(U_G, U_D) = [N_S(U_G, U_D) + P_S(U_G, U_D) + 2n_i]^{-1}. \quad (6)$$

Equation (4) shows that G is a function of U_G and U_D. The factor of A relates only to U_D and determines the G peak. The B factor determines the width of the G curve and relates to both U_D and U_G. The G is the generation rate at $G > 0$ and it is the recombination rate at $G < 0$. Figure 3 shows the simulated G based on Eq. (4). It can be seen that $G > 0$ at $U_D > 0$, and $G < 0$ at $U_D < 0$ in Fig. 3. In addition, each G curve has a peak. According to Eq. (4), the formation of G peak requires $N_S(U_G, U_D) = P_S(U_G, U_D)$. Then it is the crossover point that corresponds to the G peak G_{max}. The G_{max} can be seen to shift rightwards with increasing U_D. The U_{GF} at G_{max}, $U_{GF}(G_{max})$, can be deduced as follows:

$$U_{GF}(G_{max}) = \frac{1}{\beta} \ln \frac{N_A}{n_i} + \frac{U_D}{2} + \frac{\sqrt{2q\varepsilon_S N_A}}{C_{ox}} \left(\frac{1}{\beta} \ln \frac{N_A}{n_i} + \frac{3}{2} U_D \right)^{1/2}. \quad (7)$$

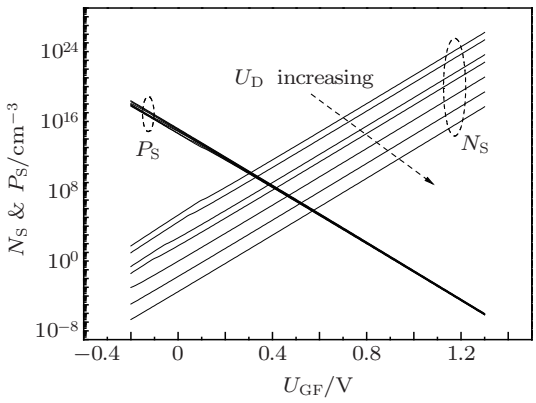


Fig. 2. Simulated N_S and P_S as a function of U_{GF}. U_D increases from −0.1 V, −0.05 V, 0.05 V, 0.1 V, 0.2 V, 0.3 V to 0.4 V. In simulation $t_{ox} = 4$ nm and the substrate doping $N_A = 5 \times 10^{15}$ cm^{-3}, respectively.

Substituting Eq. (7) into Eq. (4), G_{max} can be deduced as

$$G_{max} = n_i[1 - \exp(-\beta U_D/2)]/2. \quad (8)$$

Further, the full width at half maximum (FWHM) value of G_{max}, U_{G-h}, can be used to describe the scope of the G curve. When $G = G_{max}/2$, then equation (4) becomes

$$G_{max}/2 = A(U_D) \times B(U_G, U_D) n_i^2. \quad (9)$$

Solving Eq. (9), the interface electron density N_{S-h} and hole density N_{S-h} at $G = G_{max}/2$ can be expressed as

$$N_{S-h} + P_{S-h} = 2n_i[1 + 2\exp(-\beta U_D/2)]. \quad (10)$$

It is the relationship of $(N_S + P_S)$ versus U_{GF} that can be extracted from Fig. 2, as shown in Fig. 4(a). Each $(N_S + P_S)$ curve presents a V-shape-like curve. The peak of the V-shape is located at $N_S = P_S$, which is the crossover of N_S and P_S in Fig. 2. The $(N_{S-h} + P_{S-h})$ curves based on Eq. (10) are also shown in Fig. 4(a) and they intersect the curves of $(N_S + P_S)$. The range of U_{GF} between the two crossover points is U_{G-h}. The relationship of U_{G-h} with U_D is given in Fig. 4(b). In the reverse mode ($U_D > 0$ V), U_{G-h} is linear with respect to U_D and the slope is about 0.95. On the basis of the above analysis, the increase of U_{G-h} results in the extension of the G curve with increasing U_D. For the case of forward mode ($U_D < 0$ V), the relationship between U_{G-h} and U_D is very weak, as shown in Fig. 4(b). This does not accord with the scenario in Fig. 3 that G curves are extended so much as U_D varies from −0.05 V to −0.1 V. This results from the increase of G_{max} in the forward mode. For G under $U_D < 0$ V, the U_{GF} at G_{max} decreases with increasing $|U_D|$, which makes the G curve shift leftwards, as seen in Fig. 3.

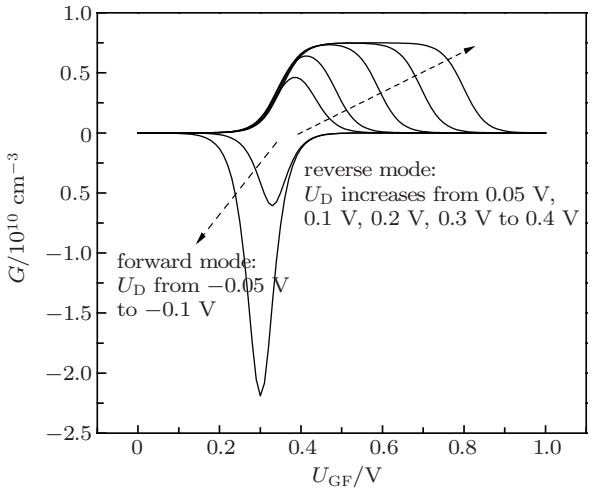


Fig. 3. Comparison of simulated line shapes of G between reverse and forward drain PN junction bias modes. The subtract doping and t_{ox} are the same as those in Fig. 2.

Then, the generation–recombination current I_{GMGR} is obtained by integrating G. Assuming that the traps are uniform along the channel interface, then I_{GMGR} will be expressed as

$$I_{GMGR} = qw\tau^{-1} \int_0^l G(N_S, P_S)\,dx = qw\tau^{-1} n_i^2 \times \int_0^l A \times B\,dx = qwl\tau^{-1} n_i^2 A \times B. \quad (11)$$

The lifetime of a carrier is given by $\tau = 1/(\sigma v_{th} N_{it})$,[15] where N_{it} is the density of interface traps, v_{th} is the thermal velocity, and σ is the capture cross section. In Eq. (11), w and l are the width and length of the device, respectively.

So I_{GMGR} is proportional to G in Eq. (11). On the basis of N_S and P_S given by Eq. (2), the I_{GMGR} curves simulated according to Eq. (11) are shown in Fig. 5. Figure 5 also shows the experimental I_{GMGR} curves, which are from Fig. 1. Note that the simulated curves have almost the same peaks as the experimental curves under $U_D > 0$ V in Fig. 5(a). But the scope of the simulated curve at a particular U_D is smaller than

that of the experimental curve. Additionally, for the case of $U_D < 0$ V, the simulated recombination current curves have the larger peaks than the experimental curves and they mismatch each other obviously. As mentioned in Eq. (4), N_S and P_S dominate $G(N_S, P_S)$ and therefore determines I_{GMGR}. So figure 5 shows the disagreements between the simulated and experimental results, which implies that N_S and P_S given by Eq. (2) are not accurate. In fact, U_D can change not only E_{FN}, but also the other parameters in the device. Although the influence of U_D on the other parameters is weak, it still makes the simulation results of I_{GMGR} deviate from the experimental results.

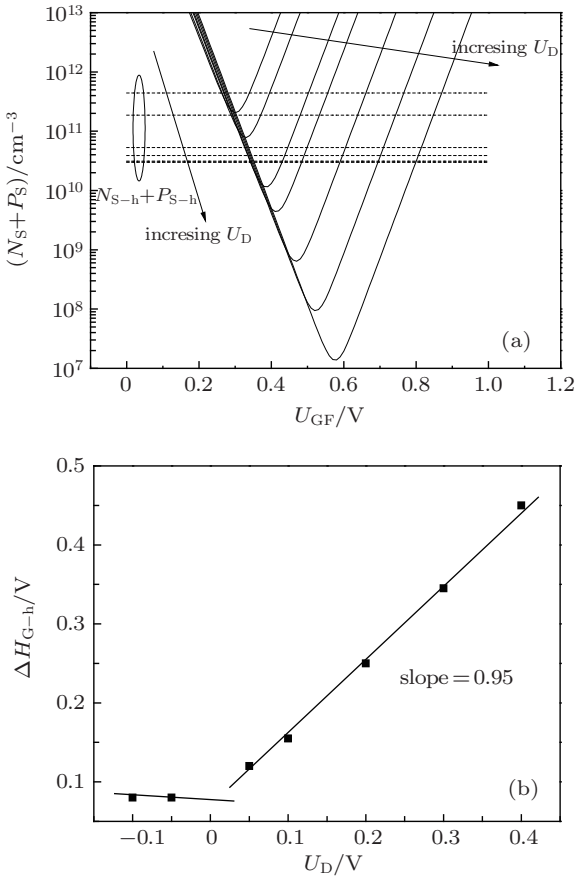


Fig. 4. (a) Variations of simulated $(N_S + P_S)$ with U_{GF}. (b) Relationship between U_{G-h} and U_D, extracted from Fig. 4(a) with $U_{FB} = -0.4$ V. The parameters in the simulation are the same as those in Fig. 2.

For the reverse mode ($U_D > 0$ V), a linear relationship exists between ΔU_{G-h} and U_D, as seen from Fig. 4(b). So it can introduce a correction factor, m, before U_D into B of Eq. (11). Parameter m can integrate the influences of all the other parameters, but cannot destroy the linear relation. Then B in Eq. (6) can be modified into

$$B(U_G, mU_D) = [N_S(U_G, mU_D) + P_S(U_G, mU_D) + 2n_i]^{-1}, \quad (12)$$

where the N_S and P_S are modified into

$$N_S(U_G, mU_D) = n_0 \exp\left\{\beta\left[\frac{q\varepsilon_s N_A}{C_{ox}^2} + U_{GF} - \frac{(2q\varepsilon_s N_A)^{1/2}}{\varepsilon_{ox}} \times \sqrt{\frac{q\varepsilon_s N_A d_{ox}^2}{2\varepsilon_{ox}} + U_{GF} + mU_D} - mU_D\right]\right\},$$

$$P_S(U_G, mU_D) = N_A \exp\left\{-\beta\left[\frac{q\varepsilon_s N_A}{C_{ox}^2} + U_{GF} - \frac{(2q\varepsilon_s N_A)^{1/2}}{\varepsilon_{ox}} \times \sqrt{\frac{q\varepsilon_s N_A d_{ox}^2}{2\varepsilon_{ox}} + U_{GF} + mU_D}\right]\right\}. \quad (13)$$

Equation (13) indicates that m can change N_S and P_S and consequently modulate B. When $m > 1$, B based on Eq. (12) becomes larger than B in Eq. (6). As a result, the I_{GMGR} curve should extend at a certain U_D. Conversely, the I_{GMGR} curve should shrink at a certain U_D when $m < 1$. Figure 5(a) shows that the simulated I_{GMGR} curve is narrower than the experimental curve, which strongly suggests that $m > 1$.

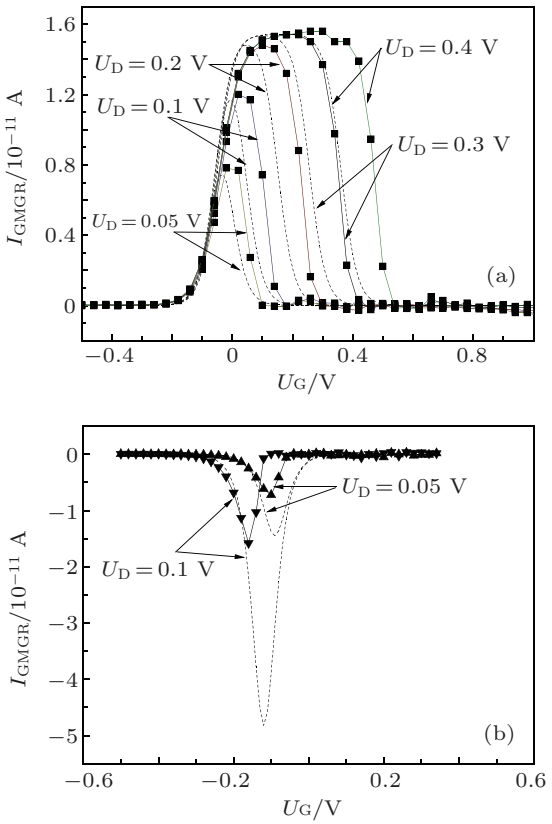


Fig. 5. Variations of experimental (symbol line) and simulated (dash line) I_{GMGR} with gate voltage U_G. (a) The generation current under $U_D > 0$ V, and (b) the recombination current under $U_D < 0$ V. In simulation $N_{it} = 2 \times 10^{11}$ cm^{-2}, $w = 0.28$ μm, and $l = 6$ μm, $\sigma = 4 \times 10^{-13}$ cm^{-2}. The other structure parameters are the same as those in Fig. 2.

Additionally, figure 5(b) shows the other problem that there is a big distinction between the peaks of I_{GMGR} between in a simulation and those in an experiment under $U_D < 0$ V. This distinction is due to A in Eq. (11) being too big because the exponent term determines A in the forward mode. So a modulating coefficient, t, can be introduced before U_D in the expression of the A factor. Then factor A becomes

$$A(tU_D) = [1 - \exp(-t\beta U_D)]. \quad (14)$$

Although the introduction of m is based on the case of $U_D > 0$ V, m can in theory shrink the recombination current curve when $U_D < 0$ V, according to Eqs. (12) and (13). The simulated curve in Fig. 5(b) just needs narrowing, so m can

meet the case of $U_D < 0$ V. As to the coefficient t, it should have little influence on factor A when $U_D > 0$ V because the exponent term can be ignored in factor A. So the introduction of t cannot affect the I_{GMGR} curve evidently. On the basis of the above analysis, it is reasonable to introduce m and t into Eqs. (12) and (14). Then substituting these two equations into Eq. (11), the modified I_{GMGR} is given by

$$\begin{aligned} I_{GMGR} &= qwl\tau^{-1}n_i^2 A(tU_D) \times B(U_G, mU_D) \\ &= qwl\tau^{-1}n_i^2[1-\exp(-t\beta U_D)] \\ &\quad \times [N_S(U_G, mU_D) + P_S(U_G, mU_D) + 2n_i]^{-1}. \end{aligned} \quad (15)$$

Figure 6 shows the comparisons between experimental I_{GMGR} curves and the simulated I_{GMGR} curves based on the model of Eq. (15). In the simulations, m and t are 1.3 and 0.85, respectively. Good agreement can be seen between the simulation results and experimental results for the cases of both $U_D > 0$ V and $U_D < 0$ V in Fig. 6. This demonstrates that the I_{GMGR} model of Eq. (15) is more accurate than that of Eq. (11). Further, it confirms that equation (15) has the universality, that is, it is applicable to reverse and forward drain PN junction bias modes.

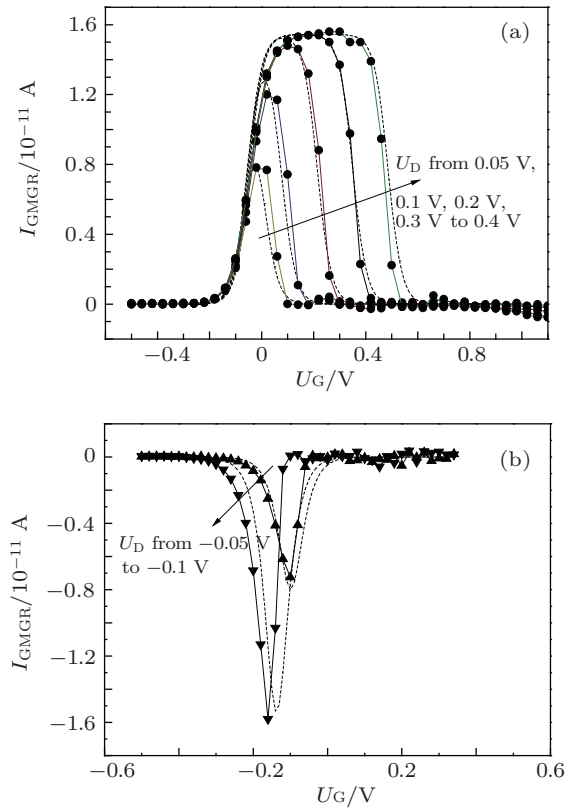


Fig. 6. (color online) The comparisons between experimental I_{GMGR} (symbol line) and simulated I_{GMGR} (dash line) according to the Eq. (15) model, (a) the generation current under $U_D > 0$ V, (b) the recombination current under $U_D < 0$ V. The parameters in the simulation are the same as those in Fig. 5.

4. Conclusions

In this paper, we investigate the characteristics of gate-modulated generation–recombination current I_{GMGR} induced by the interface traps in nMOSFET. It is found that the generation current under the reverse mode increases and the I_{GMGR} curve shifts rightwards as U_D increases. Besides, the recombination current peak under the forward mode is enhanced with increasing $|U_D|$. The variations of I_{GMGR} curves are ascribed to the changes of electron density and hole density at the interface, N_S and P_S, under the various drain bias. Based on the physical mechanism, the I_{GMGR} model is set up by introducing two coefficients m and t into A and B respectively. Coefficient m can modulate B, which can make the generation current curve expand under $U_D > 0$ V and make the recombination current curve narrow under $U_D < 0$ V. Coefficient t makes the recombination current peak diminish and has no effect on the generation current peak. The simulation results based on the I_{GMGR} model are found to agree with the experimental results very much. This model has generality, that is, it is applicable to the reverse and forward drain PN junction bias modes.

The results in this paper should be helpful to understand the gate-modulated generation–recombination current induced by interface traps and relevant reliability in nano-CMOS devices.

References

[1] Martirosian M and Ma T P 2001 *IEEE Trans. Electron Dev.* **48** 2303

[2] Rudenko T and Kilchytska V 2005 *J. Appl. Phys.* **97** 093718

[3] Speckbacher P, Berger J, Asenov A, Koch F and Weber W 1995 *IEEE Trans. Electron Dev.* **42** 1287

[4] Mori Y, Yoshimoto H, Takeda K and Yamada R 2012 *J. Appl. Phys.* **111** 104513

[5] Young C, Neugroschel A, Matthews K, Smith C, Heh D and Park H 2010 *IEEE EDL* **31** 653

[6] Bina M, Aichinger T, Pobegen G, Gos W and Grasser T 2011 *IIRW Final Report* 27

[7] Chen H F, Guo L X and Du H M 2012 *Chin. Phys. B* **21** 088501

[8] Chen H F 2013 *Acta Phys. Sin.* **62** 188503 (in Chinese)

[9] Zhang E X, Fleetwood D, Duan G X, Zhang C X, Francis S A, Duan R D, Zhang C X, Francies S A and Schrimpf R D 2012 *IEEE Trans. Nucl. Sci.* **59** 3062

[10] Ma C Y, Zhang L N, Zhang C F, Zhang X F, He J and Zhang X 2011 *Microelectronics Reliability* **51** 337

[11] Zhang C F, Ma C Y, Guo X J, Zhang X F, He J and Wang G Z 2011 *J. Semicond.* **32** 02400

[12] Hu C M 2012 *Modern Semiconductor Devices for Integrated Circuits* (Bejing: Publishing House of Electronics Industry) p. 118 (in Chinese)

[13] Sze S M 2011 *Semiconductor Devices Physics and Technology* (Suzhou: Suzhou University Press) p. 64 (in Chinese)

[14] Neamen D A 2012 *Semiconductor Physics and Devices Basic Principle* (Bejing: Publishing House of Electronics Industry) p. 159 (in Chinese)

[15] Liu E K, Zhu B S and Luo J S 1998 *Semiconductor Physics* (Xi'an: Xi'an Jiaotong University Press) p. 126 (in Chinese)